Supporting Information

Polyaniline Nanofiber Electrodes for Reversible Capture and Release of Mercury(II) from Water

Yoonseob Kim[1], Zhou Lin[1], Intak Jeon[2], Troy Van Voorhis[1], and Timothy M. Swager[1]*

1 Department of Chemistry, Massachusetts Institute of Technology, Cambridge, MA 02139 USA

2 Department of Materials Science and Engineering, Massachusetts Institute of Technology, Cambridge, MA 02139 USA

KEYWORDS. Redox-active system, polyaniline nanofiber, heavy metal ion removal, intermolecular binding energy

*To whom correspondence should be addressed. E-mail: tswager@mit.edu
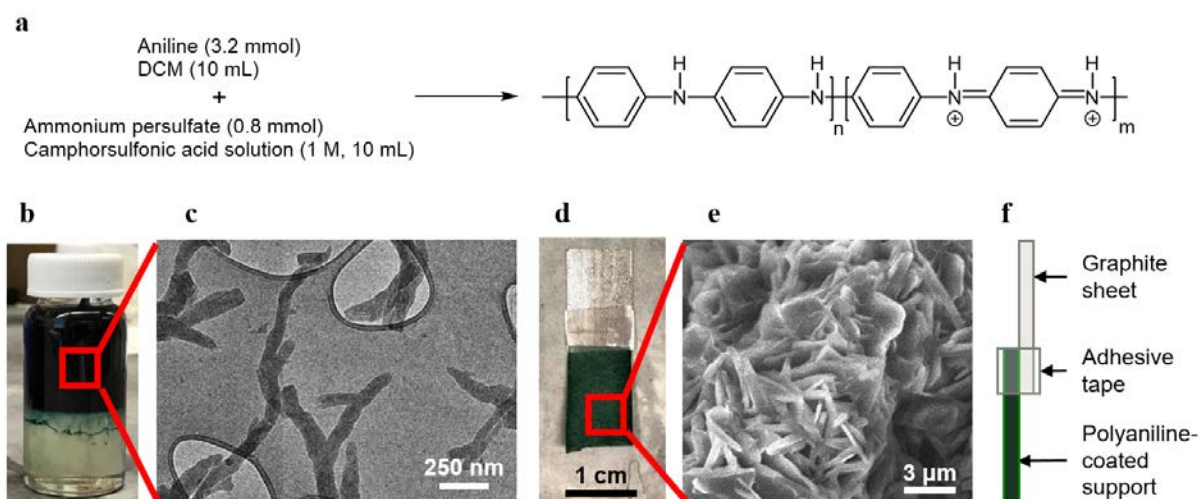
Figure S1. Preparation of PANI and PNE. a; Chemical reaction scheme for interfacial polymerization of aniline. **b;** Photographic image of interfacial polymerization of aniline, after 15 min. The top layer is an aqueous solution of 1.0 M camphorsulfonic acid and ammonium persulfate, and the bottom layer is aniline dissolved in the dichloromethane. **c;** Magnified transmission electron microscopy (TEM) images of PANI nanofibers. **d;** Photographic image of polyaniline nanofiber electrode (PNE). **e;** Scanning electron microscopy (SEM) image of the PNE's morphology. **f;** Schematic representation of a side view the PNE showing graphite sheet and polyaniline-coated absorbent were sandwiched by an adhesive tape.

Control experiment – metal ion adsorption on polypropylene substrate

The polypropylene substrates (single layer; thickness: 0.285 ± 0.053 mm, length: 30 mm, and width: 10 mm) were soaked into three stock solutions (10 mL, 1000 ppb for each of Hg^{2+}, Pb^{2+}, and Cd^{2+}) for 12 h. Then the number of ion in the solution was counted using ICP-MS. It turned out that more than 99% of the original stock solution ions were observed, meaning the polypropylene substrate is inactive toward the three cations.
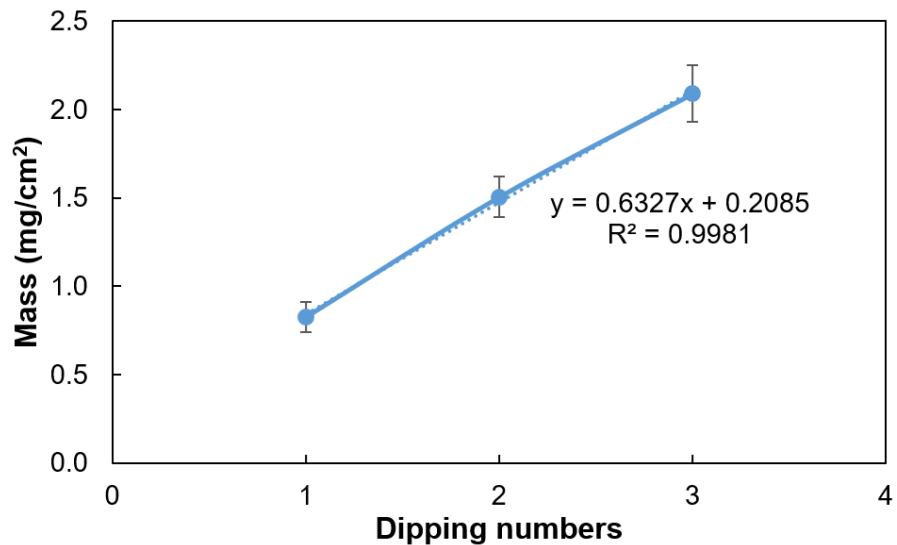
Figure S2. A linear increase of PANI mass to the dipping cycles. The amount of PANI absorbed per area by the polypropylene mat with different dipping numbers. Thickness of the mat is 0.285 ± 0.05 mm. The weight of the PANI dispersion is obtained by the weight difference of the vacuum dried sheet, before and after the soaking.
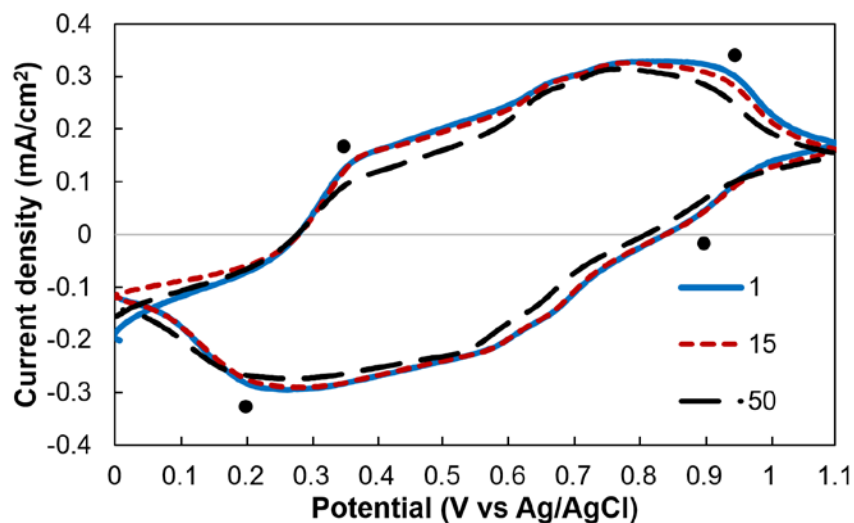
Figure S3. Stability test of PNE. Cyclic voltammograms of the PANI electrode in a monomer-free electrolyte solution, recorded in 0.5 M H_2SO_4 electrolyte solution at a scan rate of 10 mV/s with pyrolytic graphite sheet as a counter electrode.

The as-prepared PNE was evaluated for its stability by repeating the scans in 0.5 M H_2SO_4 electrolyte solution. The voltammograms obtained after 15th cycles nearly perfectly overlapped with the initial one indicating excellent mechanical stability and adhesion of PANI nanofibers onto the polypropylene substrate. The 50th cycle showed marginal decrease of the electrochemical activity.
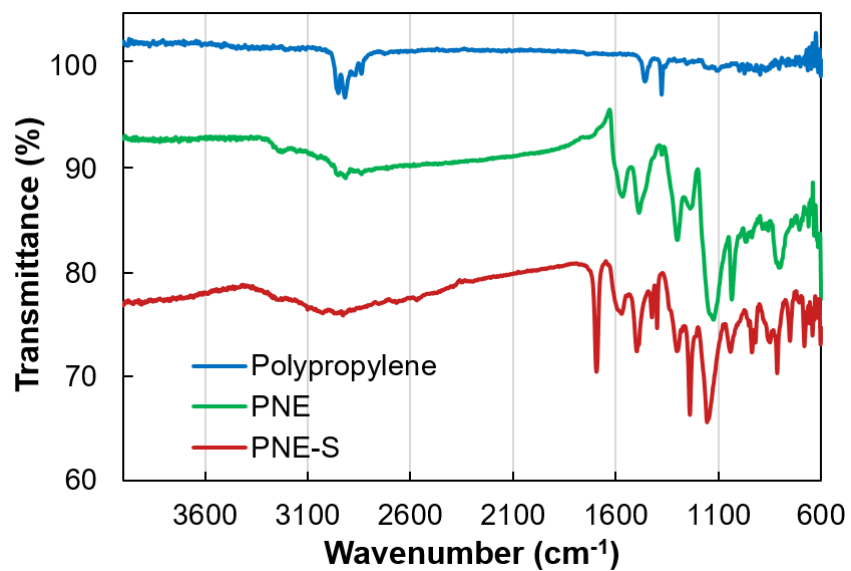
Figure S4. Fourier-transform infrared spectra of polypropylene mat, PNE and PNE-S. For PNE and PNE-S, due to the strong adhesion between the polypropylene substrate and PANI nanofibers, the samples including the polypropylene substrate were characterized.
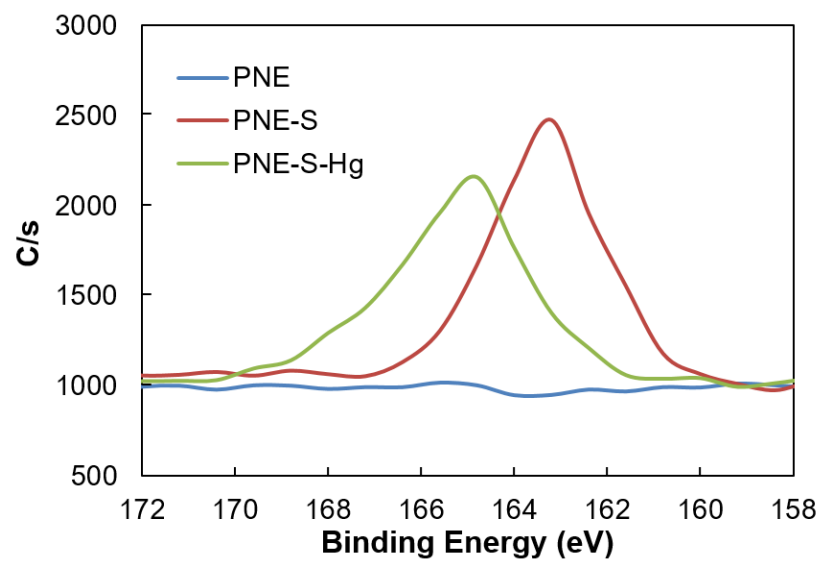
Figure S5. XPS spectra of PNE, PNE-S, and Hg^{2+} adsorbed PNE-S (PNE-S-Hg).

Effect of pH on adsorptions:

The effect of pH on Hg^{2+} removal was investigated in the ranges of 2.0 – 10.0. One PANI electrode sample was soaked into a 10 mL aqueous $Hg(NO_3)_2$ (1 ppm) with different pH values for 12 h at room temperature with gently stirred. The solution pH has an effect on the adsorption (Fig. S6). The two curves present similar trends with apparent suppression observed in both alkaline and highly acidic solutions. The optimum pH range is 4.0 - 6.0 for both PNE and PNE-S. The corresponding maximum adsorption percentages are 89.6 and 99.9 %, respectively. At low pH ranges 2.0 - 4.0, the reduced adsorption is likely due to protonation of functional groups resulting low attachment of Hg^{2+}. The adsorption percentage increased with increasing pH and reached almost maximum around pH = 6. The de-protonation of the functional groups on adsorbent should result in the increased uptake of Hg^{2+}. The adsorption capacity was then maintained at about the same level within the pH range of 5.0 - 6.0. Further increasing the pH above 6 decreased the adsorption, presumably due to interactions between OH^- and Hg^{2+} forming $Hg(OH)^+$ $Hg(OH)_2$ species. This observed adsorption of Hg^{2+} is consistent with reported results.[1]
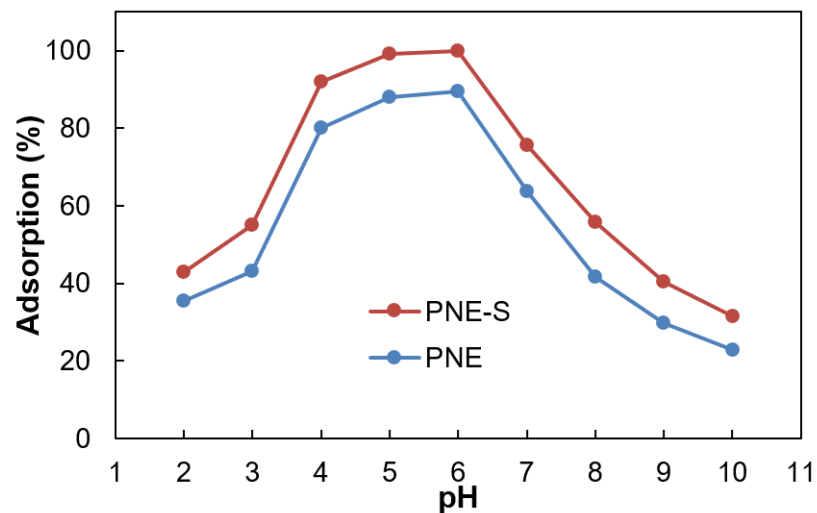
Figure S6. Effect of pH on Hg^{2+} adsorption by PNE-S and PNE. PNE-S and PNE were soaked in 10 mL of 1000 ppb Hg^{2+} solution for 12 h at room temperature. pH was adjusted by HNO$_3$ and NaOH solutions.
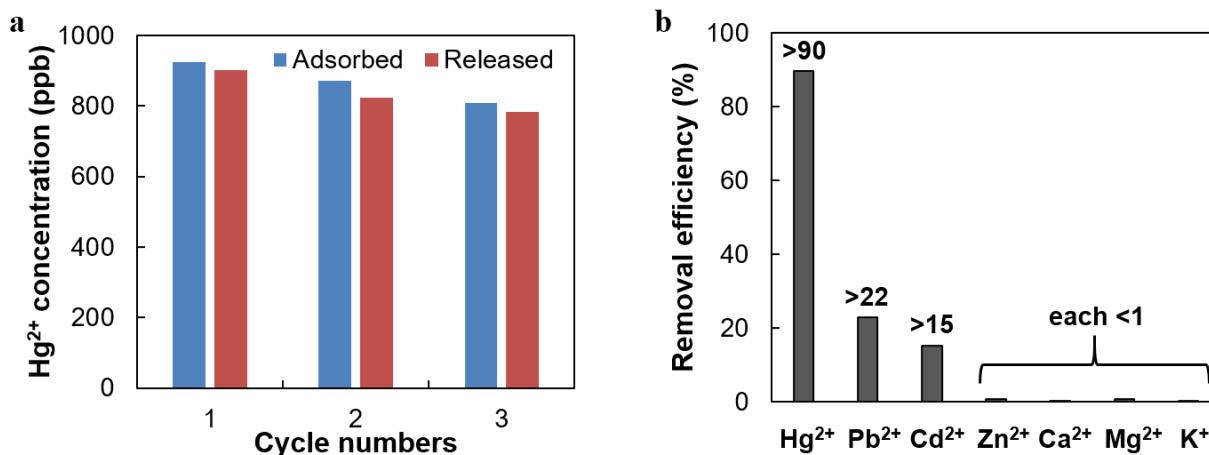
Figure S7. Recyclability and selectivity test of PNE. a; Recycle use of PNE for facile capture and release of Hg^{2+}. Adsorption performed by soaking the electrode into the ion-containing solution for 12 h. Application of fixed oxidation potential at 0.5 V vs Ag/AgCl results in Hg^{2+} release. The electrode is then placed in a fresh solution for the next adsorption cycle. **b;** Selectivity of PNE towards various cations.
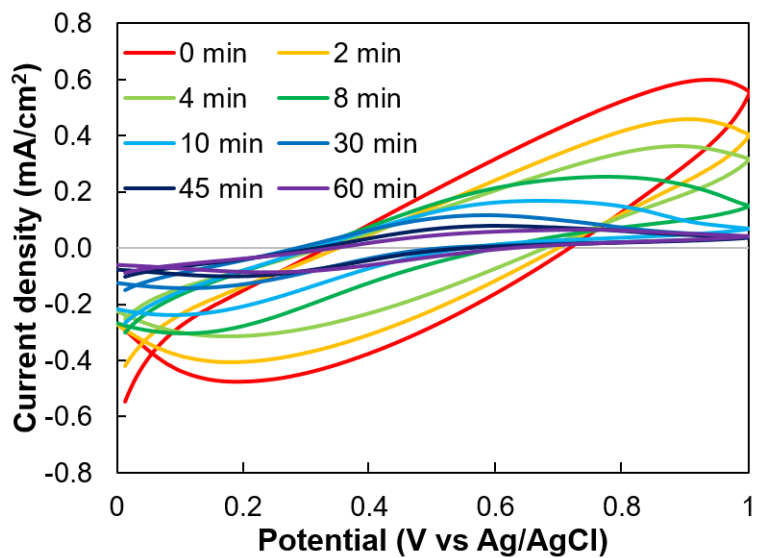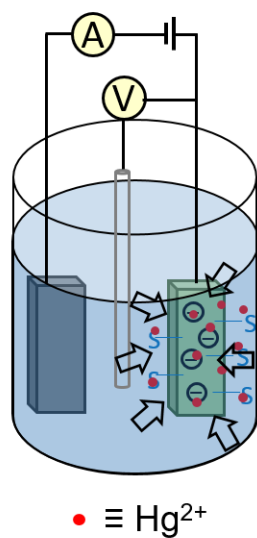
Figure S8. Hg^{2+} adsorption experiment and the related change of cyclic voltammograms of PNE-S, measured in a series of time sequence. Cyclic voltammograms were recorded in 0.5 M H$_2$SO$_4$ electrolyte solution at a scan rate of 10 mV/s with pyrolytic graphite sheet as a counter electrode.

Computational details for DFT calculations, MD simulations and QM/MM calculations in the aqueous solution

To study the interaction between PANI and adsorbed metal ions, we constructed the minimal model system with a PANI tetramer, a metal ion (M^{n+}), several chloride anions (Cl^-) to balance the charge, as well as sufficient water molecules as the explicit solvent. Three PANI tetrameric species were computationally investigated in the present study, including one that maintains the original reduced state and two oxidized ones with one and two electrons removed, respectively. These three species provide the simplest descriptions for leucoemeraldine, emeraldine, and pernigraniline, respectively.

The geometries of all three isolated PANI tetrameric species were optimized using the B3LYP[2,3]+D3[4] exchange-correlation functional at the 6-31G* level in Q-Chem 5.0.[5] All these states show low-barrier internal rotations along C-N bonds (Fig. S9) and prefer twisted configurations. To facilitate subsequent MD simulations, the atomic partial charges of all three PANI tetramers were evaluated based on the CHarges from ELectrostatic Potentials using a Grid-based (CHELPG)[6] method at the same level of theory in Q-Chem 5.0.

(a) PANI(0)   (b) PANI(I)   (c) PANI(II)
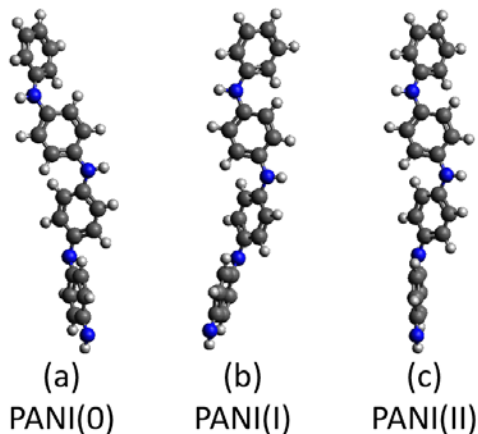
Figure S9. Optimized geometries of isolated PANI tetramers in the (a) reduced state and the oxidized states with (b) one, and (c) two electrons removed, evaluated using gas-phase DFT calculations.

We then sampled the configurations of PANI-M^{n+} complexes using the solution-phase MD simulations in GROMACS 5.1.[7] The CHELPG atomic charges of the PANI tetramers were implemented as a modification to the latest OPLS/AA force field.[8,9] Also, Lennard-Jones[10] parameters of Cd^{2+}, Hg^{2+}, and Pb^{2+} were obtained from literature and added to the OPLS/AA force field (Table S1). The initial configurations of the simulation systems were generated in Packmol[11] by randomly placing one M^{n+} ion, sufficient Cl^- anions, and 2115 water molecules around the PANI tetramer, and were contained in a cubic box with a 4 nm length with periodic boundary conditions (PBC) on all surfaces. The energy minimizations were performed to optimize initial configurations using the steepest descent algorithm with a minimum energy step size of 0.01 kJ mol^{-1} and a maximum force of 10 kJ mol^{-1} nm^{-1}. The *NVT* simulations (constant number (N), volume (V), and temperature (T)) were performed at 298 K using a Nose−Hoover thermostat for 1 ns at the time step of 1 fs to equilibrate the systems, followed by the production simulations for another 1 ns.

Table S1. Parameters in the Lennard-Jones potential, $V_{LJ} = 4\varepsilon[(\sigma/r)^{12} - (\sigma/r)^{6}]$.

Metal ion	ε (kJ mol^{-1})	σ (nm)	Ref.
Cd^{2+}	0.197	0.276	12
Hg^{2+}	4.090	0.250	13
Pb^{2+}	12.259	0.318	14

The interactions between PANI and M^{n+} were analyzed for all three oxidation states based on the results of MD simulations. We extracted 200 snapshots from the production run of each species. The configuration of one representative snapshot is provided in Fig. S10 for each metal ion. For each snapshot, we evaluated the binding energy (E_{bind}) between the PANI tetramer and M^{n+} following Eq. 1 in the main text. $E(PANI)$, $E(M^{n+})$ and $E(PANI−M^{n+})$ were evaluated using the hybrid QM/MM[15] approach, in which the system (PANI and/or M^{n+}) was treated using DFT at the B3LYP+D3/6-31G* level, and the environment (Cl^- and water) was treated using MM based

on the OPLS/AA force field modified by us. E(PANI) and $E(M^{n+})$ were evaluated using ground-state DFT and E(PANI-M^{n+}) was evaluated using constrained DFT (CDFT)[16] which can specify the charges of PANI and M^{n+} to agree with their isolated counterparts so that the unphysical electron transfer between PANI and M^{n+} was forced not to occur. All QM/MM calculations reported in the present study were performed using Q-Chem 5.0.

The statistical results of E_{bind} for all snapshots are summarized in Fig. 3 in the main text, and their histograms are also provided in Fig. S11. Our evaluations show that the reduced PANI tetramer can selectively bind to Hg^{2+} in the aqueous environment (largest positive E_{bind}), while its oxidation can reverse this binding process and release these ions (negative E_{bind}).
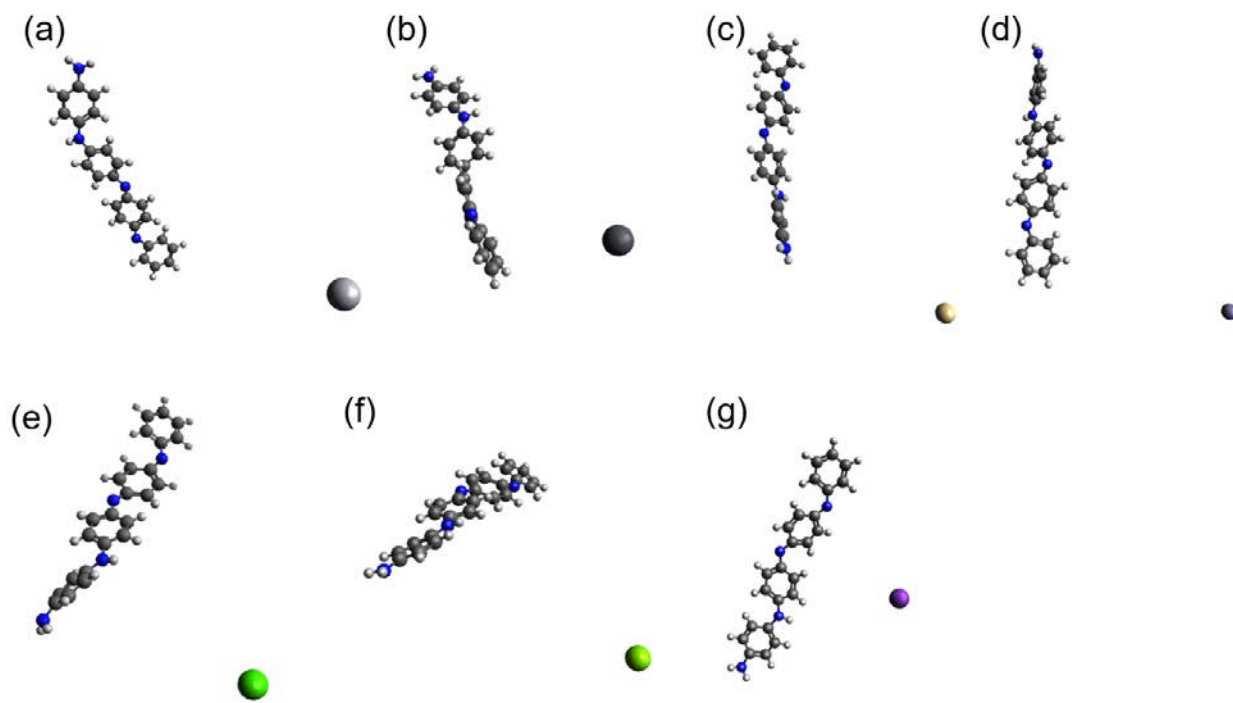
Figure S10. Representative configurations of the PANI(0)-M^{n+} complexes (M^{n+} = (a) Hg^{2+}, (b) Pb^{2+}, (c) Cd^{2+}, (d) Zn^{2+}, (e) Ca^{2+}, (f) Mg^{2+}, and (g) K^+) that were used to evaluate binding energies. These structures were obtained from the first snapshot of each production MD trajectory and are only illustrated here as representative examples.
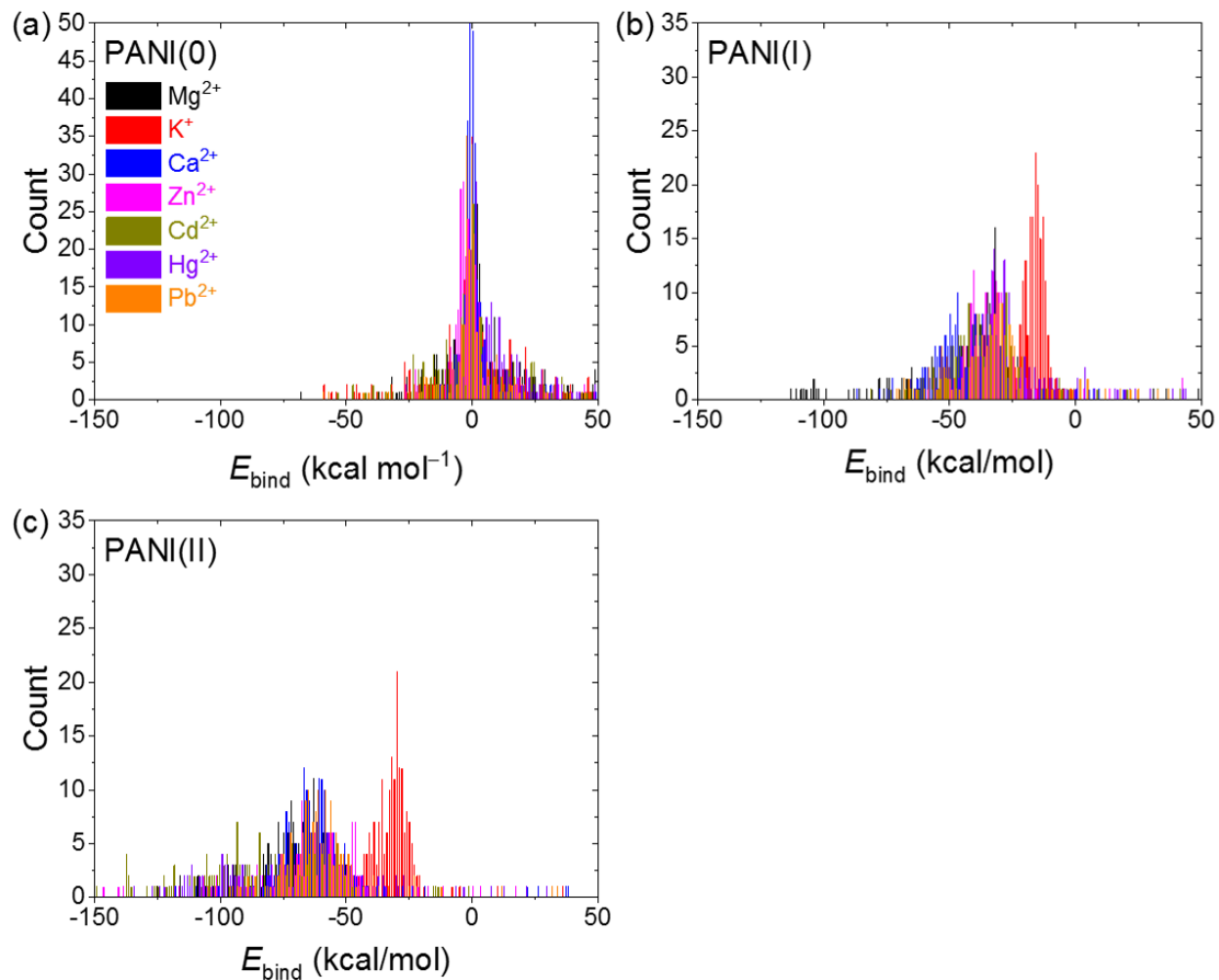
Figure S11. Histograms of binding energies (E_{bind}) between the PANI tetramer and the metal ions in the aqueous solutions sampled using MD and evaluated using CDFT-based QM/MM.
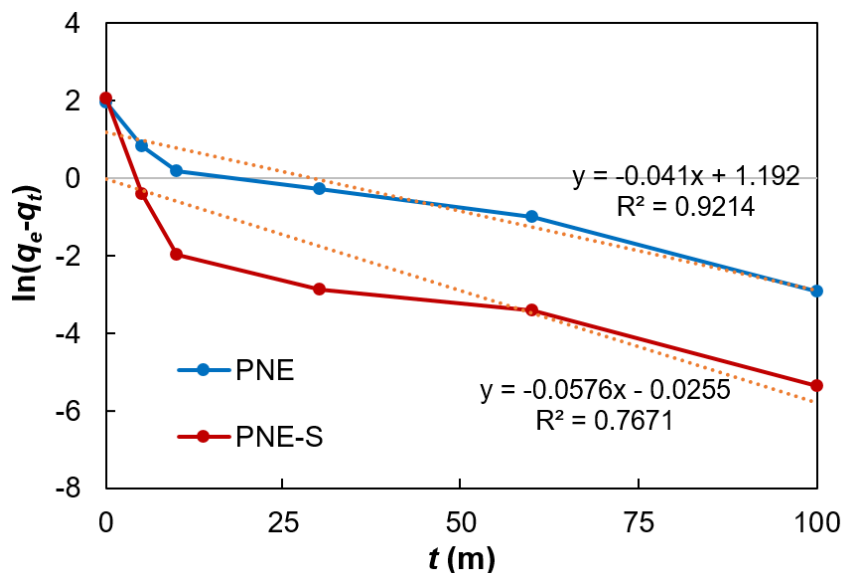
Figure S12. Fitting kinetic data to pseudo-first-order kinetic model.

As can be seen from the R^2 values, nanofiber electrodes had weaker correlation to the pseudo-first-order kinetic model, indicating that physisorption is not a significant step. Below is the pseudo-first-order kinetic equation:

$$\ln(q_e - q_t) = \ln q_e - k_1 t \qquad (\text{Eq. S1})$$

where, q_t, q_e (mg g^{-1}) are the amount of mercury ion adsorbed (mg g^{-1}) at time t and equilibrium (min), k_1 (min^{-1}) is the rate constant of the model.

Table S2. Comparison of q_m and k_2 of various polyaniline adsorbents.

Benchmark materials	Morphology of polyaniline	k_2 (g mg^{-1} min^{-1})	q_m (mg g^{-1})	Ref.
Polyaniline/humic acid nanocomposite	Aggregated spherical particles	3.08×10^{-4}	671	27 in the main text
Polyaniline/reduced graphene oxide (RGO)	Tiny polyaniline grown on layered RGO	1.21×10^{-4}	1,000	45 in the main text
polyaniline/attapulgite composite	Homogeneous coating on substrate (but detail unknown)	2.90×10^{-4}	824	23 in the main text
polyaniline/cellulose acetate composite	Mix of fiber and particle	6.92×10^{-5}	280	22 in the main text
polyaniline microspheres	Microspheres	7.5×10^{-3}	155	44 in the main text
Aniline/Sulfoanisidine Copolymer	Nanoparticles	1.185×10^{-4}	2,070*	40 in the main text

k_2 and q_m value referred herein were measured based on the similar stock solution concentrations up to 500 ppm. However, the value ($q_m = 2,070$ mg g^{-1}) was obtained with stock solution concentration ranges up to 16,000 ppm, which is unusually high.*

Table S3. Comparison of q_m and k_2 of various adsorbents, not including polyaniline.

Benchmark materials	k_2	K_d	q_m	Ref.
	(g mg^{-1} min^{-1})	(mL g^{-1})	(mg g^{-1})	
Porous organic polymers, thiol-functionalized	8.13	5.76×10^7	1,014	13 in the main text
Mesoporous carbon, sulfur-functionalized	(unknown)	5.13×10^5	732	46 in the main text
Metal organic framework, thiol-functionalized	1.3×10^{-1}	4.73×10^5	714	17
Metal organic framework, acylamide- & hydroxyl-functionalized	1.2×10^{-1}	(unknown)	333	18
Covalent organic framework, thiol functionalized	(unknown)	2.3×10^9	1,350	20 in the main text
Covalent organic framework, thiol grafted imine-based	11.5	3.23×10^9	4,395	21 in the main text
Covalent organic framework, thioether functionalized	6.31	7.82×10^5	734	18 in the main text
Hydrogen metal sulfide	(unknown)	6.4×10^6	87	19
Aerogel from chalcogenide	(unknown)	1.6×10^7	645	11 in the main text
Mesoporous silica	(unknown)	3.4×10^5	(unknown)	20

References

(1)   Wang, J.; Deng, B.; Chen, H.; Wang, X.; Zheng, J. *Environ. Sci. Technol.* **2009**, *43*, 5223.

(2)   Becke, A. D. *J. Chem. Phys.* **1993**, *98*, 5648.

(3)   Lee, C.; Yang, W.; Parr, R. G. *Phys. Rev. B* **1988**, *37*, 785.

(4)   Grimme, S. *J. Comput. Chem.* **2006**, *27*, 1787–1799.

(5)   Shao, Y.; Gan, Z.; Epifanovsky, E.; Gilbert, A. T. B.; Wormit, M.; Kussmann, J.; Lange, A. W.; Behn, A.; Deng, J.; Feng, X.; et al. *Mol. Phys.* **2015**, *113*, 184.

(6)   Breneman, C. M.; Wiberg, K. B. *J. Comput. Chem.* **1990**, *11*, 361.

(7)   Pronk, S.; Páll, S.; Schulz, R.; Larsson, P.; Bjelkmar, P.; Apostolov, R.; Shirts, M. R.; Smith, J. C.; Kasson, P. M.; Van Der Spoel, D.; et al. *Bioinformatics* **2013**, *29*, 845.

(8)   Wang, L. P.; Martinez, T. J.; Pande, V. S. *J. Phys. Chem. Lett.* **2014**, *5*, 1885.

(9)   Robertson, M. J.; Tirado-Rives, J.; Jorgensen, W. L. *J. Chem. Theory Comput.* **2015**, *11*, 3499.

(10)   Jones, J. E. *Proc. R. Soc. A Math. Phys. Eng. Sci.* **1924**, *106*, 463–477.

(11)   Martinez, L.; Andrade, R.; Birgin, E. G.; Martínez, J. M. *J. Comput. Chem.* **2009**, *30*, 2157.

(12)   Dezfoli, A. A.; Mehrabian, M. A.; Hashemipour, H. *Chem. Eng. Commun.* **2015**, *202*, 1685.

(13)   Šebesta, F.; Sláma, V.; Melcr, J.; Futera, Z.; Burda, J. V. *J. Chem. Theory Comput.* **2016**, *12*, 3681.

(14)   Heinz, H.; Vaia, R. A.; Farmer, B. L.; Naik, R. R. *J. Phys. Chem. C* **2008**, *112*, 17281.

(15)   Warshel, A.; Levitt, M. *J. Mol. Biol.* **1976**, *103*, 227.

(16)   Wu, Q.; Van Voorhis, T. *J. Phys. Chem. A* **2006**, *110*, 9212.

(17)   Ke, F.; Qiu, L.-G.; Yuan, Y.-P.; Peng, F.-M.; Jiang, X.; Xie, A.-J.; Shen, Y.-H.; Zhu, J.-F. *J. Hazard. Mater.* **2011**, *196*, 36.

(18)   Luo, F.; Chen, J. L.; Dang, L. L.; Zhou, W. N.; Lin, H. L.; Li, J. Q.; Liu, S. J.; Luo, M. B. *J. Mater. Chem. A* **2015**, *3*, 9616.

(19)   Manos, M. J.; Petkov, V. G.; Kanatzidis, M. G. *Adv. Funct. Mater.* **2009**, *19*, 1087.

(20)   Feng, X.; Fryxell, G. E.; Wang, L.-Q.; Kim, A. Y.; Liu, J.; Kemner, K. M. *Science.* **1997**, *276*, 923.